

Constraints on local primordial non-Gaussianity from large scale structure

Anže Slosar,¹ Christopher Hirata,² Uroš Seljak,^{3,4} Shirley Ho,⁵ and Nikhil Padmanabhan⁶

¹*Berkeley Center for Cosmological Physics, Physics Department and Lawrence Berkeley National Laboratory, University of California, Berkeley California 94720, USA*

²*Caltech M/C 130-33, Pasadena, California 91125, USA*

³*Institute for Theoretical Physics, University of Zurich, Zurich, Switzerland*

⁴*Physics Department, University of California, Berkeley, California 94720, USA*

⁵*Department of Astrophysical Sciences, Peyton Hall,*

Princeton University, Princeton, New Jersey 08544, USA

⁶*Lawrence Berkeley National Laboratory, University of California, Berkeley CA 94720, USA*

(Dated: November 26, 2024)

Recent work has shown that the local non-Gaussianity parameter f_{NL} induces a scale-dependent bias, whose amplitude is growing with scale. Here we first rederive this result within the context of peak-background split formalism and show that it only depends on the assumption of universality of mass function, assuming halo bias only depends on mass. We then use extended Press-Schechter formalism to argue that this assumption may be violated and the scale dependent bias will depend on other properties, such as merging history of halos. In particular, in the limit of recent mergers we find the effect is suppressed. Next we use these predictions in conjunction with a compendium of large scale data to put a limit on the value of f_{NL} . When combining all data assuming that halo occupation depends only on halo mass, we get a limit of -29 (-65) $< f_{\text{NL}} < +70$ ($+93$) at 95% (99.7%) confidence. While we use a wide range of datasets, our combined result is dominated by the signal from the SDSS photometric quasar sample. If the latter are modelled as recent mergers then the limits weaken to -31 (-96) $< f_{\text{NL}} < +70$ ($+96$). These limits are comparable to the strongest current limits from the WMAP 5 year analysis, with no evidence of a positive signal in f_{NL} . While the method needs to be thoroughly tested against large scale structure simulations with realistic quasar and galaxy formation models, our results indicate that this is a competitive method relative to CMB and should be further pursued both observationally and theoretically.

PACS numbers: 98.80.Jk, 98.80.Cq

I. INTRODUCTION

The origin of structure formation in the universe is one of the most hotly debated topics in current cosmology research. The standard paradigm is that of inflation [1, 2, 3, 4], which has been tremendously successful in describing a very large number of very distinct data-sets (see e.g. [5]). Inflationary models generically predict a flat universe and nearly scale-invariant spectrum of initial fluctuations [6, 7, 8, 9, 10], both of which seem to be confirmed by observations. Consequently, a lot of effort is being put into constraining observables that might actually distinguish between different models of inflation. At the moment, this is done as a multi-pronged effort: first, measurement of the primordial power spectrum gives a direct measure of the inflationary potential shape and inflationary models differ on the actual slope, some predicting red and some blue spectrum. Moreover, inflation predicts that the primordial slope should only be changing with scale very slowly and any deviation from this prediction would be a surprise in need of an explanation. Second, a detection of B -mode polarization in the cosmic microwave background, if interpreted as gravitational waves from the early Universe, will effectively determine the energy scale of inflation and rule out a major class of inflationary models that predict inflation occurs at a low energy scale [11]. Alternatives to inflation, such as ekpyrotic models [11, 12, 13, 14], differ from inflation-

ary predictions in that the expected gravitational wave signal in CMB is always negligible. Thus, they can be falsified if primordial gravitational waves are detected. Third, multifield models could generate isocurvature perturbations; while now ruled out as the main mode of structure formation, these could be present at a subdominant level and if detected would rule out the simplest models of inflation [15, 16, 17, 18].

A fourth direction, and the one we focus on in this paper, is non-Gaussianity in initial conditions. Standard single field inflation predicts that the departures from Gaussianity are very small and not accessible to the current observational constraints. Most of the models predict that non-Gaussianity is of the local type, meaning that it depends on the local value of the potential only. A standard parameterization of the primordial non-Gaussianity is the so-called scale-independent f_{NL} parameterization, in which one includes a quadratic correction to the potential [19, 20]:

$$\Phi = \phi + f_{\text{NL}}\phi^2, \quad (1)$$

where ϕ is the primordial potential assumed to be a Gaussian random field and f_{NL} describes the amplitude of the correction. A typical value of f_{NL} for standard slow roll inflation is of the order of slow roll parameter and thus of order 10^{-2} [21], but this is likely to be swamped by the contribution from nonlinear transformation between the primordial field fluctuation (assumed to be Gaussian

if it started from the pure Bunch-Davies vacuum) and the observable (such as CMB temperature fluctuation), which generically gives f_{NL} of order unity (see e.g. [22]). Models where f_{NL} is significantly higher include multi-field inflation [23, 24, 25] as well as models where non-Gaussianity arises during reheating [26, 27] or preheating [28, 29, 30, 31]. Non-slow roll inflation models may also lead to a significant non-Gaussianity, but are constrained because they may not lead to enough inflation in the first place. Note that since $\phi \sim 10^{-5}$ even $f_{\text{NL}} \sim 100$, comparable to the present limits, generates non-Gaussian signatures only at a 10^{-3} level, so the non-Gaussian signal one is searching for is very small. Overall, any detection of f_{NL} above unity would be a major surprise in need of an explanation within the inflationary paradigm.

Very recently, non-Gaussianity in ekpyrotic models has also been studied with the results suggesting that non-Gaussianity in these models is generically large [32] and often correlated with the spectral slope n_s [33, 34], in the sense that the redder the spectrum the higher non-Gaussianity one may expect. Thus, non-Gaussianity is emerging as one of the strongest discriminators among the models attempting to explain the origins of structure in the universe.

Traditionally, the cleanest method for detecting the non-Gaussianity has been to measure the bispectrum or 3-point function of the Cosmic Microwave Background (CMB). The initial 3-year Wilkinson Anisotropy Probe (WMAP) result gave a limit on f_{NL} of $-54 < f_{\text{NL}} < 134$ [35] (all limits reported at 95% confidence limit) from the bispectrum of the WMAP data at $\ell < 400$. This has been improved subsequently to $-36 < f_{\text{NL}} < 100$ by the 3 year analysis [36]. However, Yadav & Wandelt recently claimed a detection of $f_{\text{NL}} > 0$ at 99.5% significance, with 2σ range $27 < f_{\text{NL}} < 147$ [?]. This result is surprising as, taken at its face value, it implies a very non-standard inflation or something else all together. Interestingly, a similar result has been obtained by Jeong & Smoot using the one-point distribution function of the CMB [38]. The WMAP 5-year results also prefer positive f_{NL} from their bispectrum analysis, although zero f_{NL} is within its 2-sigma significance [5], namely $-9 < f_{\text{NL}} < 111$.

An alternative method that has been applied to CMB are Minkowski functionals [35]. WMAP 3-year analysis via this technique puts the limit at $-70 < f_{\text{NL}} < 91$ [39], while the recent WMAP 5-year analysis gives $-178 < f_{\text{NL}} < 64$ from Minkowski functionals, which is about a factor of two larger error than from bispectrum analysis [5].

In the near future, the Planck satellite should improve these numbers significantly and can in principle push to $\sigma(f_{\text{NL}}) \sim 7$ [40], while more speculatively, the pre-ionization H I 21 cm transition may offer an unprecedented access to the 3-dimensional distribution of linear modes at high redshift and may bring us into regime $\sigma(f_{\text{NL}}) \ll 1$ where a detection is expected [41].

A different direction to probe non-Gaussianity is to try and determine what observational signatures it leaves in

the large scale structure (LSS) of the universe. The main problem is that non-linearities add their own phase correlations between Fourier modes that can very quickly swamp the primordial signal. Historically, the focus was on the mass function of very massive virialised structures [42, 43, 44, 45, 46]. The motivation was the notion that very massive virialised objects correspond to very rare peaks in the initial density field and therefore their number density should be an exponentially sensitive probe of those peaks at the high mass end, allowing a unique probe of the primordial peak structure. While results generally agree with this picture, the observational task is made very difficult by the low number statistics of such objects, uncertainties in the mass-observable relation and its scatter, and selection effects.

A different method has been recently proposed by Dalal et al. [47]. By extending the classical calculation for calculating the clustering of rare peaks in a Gaussian field [48] to the f_{NL} -type non-Gaussianity, they have shown that clustering of rare peaks exhibits a very distinct scale-dependent bias on the largest scales. The analytical result has been tested using N -body simulations, which confirm this basic picture.

The purpose of this paper is two-fold, first to provide a better theoretical understanding of the effect and the range of its applicability, and second, to apply it to the real data. We begin in Section II by providing a new, more general, derivation of the nonlinear bias induced by non-Gaussianity, highlighting more clearly its underlying assumptions. We then extend the basic derivation using the extended Press-Schechter formalism and show that for certain classes of halos, such as those that have undergone a recent merger, the results may be substantially modified.

We then use this formalism and apply it to a wide selection of publicly available large scale structure data. In Sections III–IV we discuss the data, methodology, main results and systematic issues, including application of Section II to the derived observational constraints. In Section V we discuss the results and present some directions for the future.

II. THEORY

In this section we provide theoretical derivations of the large scale bias induced by non-Gaussianity of the local type. We first derive an expression that depends only on the halo mass function and halo bias, using the fact that f_{NL} causes a local re-scaling of the amplitude σ_8 . This derivation is more general than that of Dalal et al. [47], since it is not tied to the spherical collapse model. In particular, we show that any universal mass function, such as the Sheth & Tormen mass function [49] or Press-Schechter mass function [50], leads to the equation first derived in Dalal et al. [47]. We then extend the derivation to the extended Press-Schechter (ePS) type of analysis and derive the effect of halo merger bias on Δb . Fi-

nally we comment on the accuracy of the ePS prediction and compare it to previously published N -body results.

A. Local non-Gaussianity in peak-background formalism

Large-scale bias of haloes is usually treated in the context of the peak-background split [51]. One can split the density field into a long-wavelength piece δ_l and a short-wavelength piece δ_s as in

$$\rho(\mathbf{x}) = \bar{\rho}(1 + \delta_l + \delta_s). \quad (2)$$

The local Lagrangian number density of haloes $n(\mathbf{x})$ (i.e. number density of haloes per unit halo mass) at position \mathbf{x} can then be written as a function of the local value of the long-wavelength perturbation $\delta_l(\mathbf{x})$ and the statistics of the short-wavelength fluctuations $P_s(k_s)$. The sufficiently averaged local density of halos follows the large scale matter perturbations

$$n(\mathbf{x}) = \bar{n}(1 + b_L \delta_l) \quad (3)$$

and so the Lagrangian bias is then

$$b_L = \bar{n}^{-1} \frac{\partial n}{\partial \delta_l}. \quad (4)$$

For Eulerian space bias one needs to add the Eulerian space clustering, so the total or Eulerian bias is $b = b_L + 1$. This argument leads to a generically scale-independent bias at sufficiently large scales. The specific function $b(M)$ is obtained by constructing a specific function $n[\delta_l(\mathbf{x}), P_s(k_s); M]$, generally fit to simulations, and then differentiating it.

The non-Gaussian case is complicated by the fact that large and small-scale density fluctuations are no longer independent. Instead, in the f_{NL} prescription, one may separate long- and short-wavelength Gaussian potential fluctuations,

$$\phi = \phi_l + \phi_s, \quad (5)$$

which are independent. Inserting into Equation (1) we can then re-map these into the non-Gaussian potential fluctuations,

$$\Phi = \phi_l + f_{\text{NL}}\phi_l^2 + (1 + 2f_{\text{NL}}\phi_l)\phi_s + f_{\text{NL}}\phi_s^2 + \text{const.} \quad (6)$$

We can then convert this to a density field using the expression $\delta_l(k) = \alpha(k)\Phi(k)$, with

$$\alpha(k) = \frac{2c^2 k^2 T(k) D(z)}{3\Omega_m H_0^2}. \quad (7)$$

Here $T(k)$ is the transfer function, c speed of light, $D(z)$ the linear growth factor normalised to be $(1+z)^{-1}$ in the matter domination, Ω_0 the matter density today and H_0 the Hubble parameter today. The operator $\alpha(k)$ makes

it non-local on scales of ~ 100 Mpc, so this can also be thought of as a convolution operator in real space.

For long-wavelength modes of the density field, one may write

$$\delta_l(k) = \alpha(k)\phi_l(k); \quad (8)$$

the remaining terms in Equation (6) are either much smaller ($f_{\text{NL}}\phi_l^2$), have only short-wavelength pieces $[(1 + 2f_{\text{NL}}\phi_l)\phi_s]$, or simply add a small white noise contribution on large scales ($f_{\text{NL}}\phi_s^2$).

Within a region of given large-scale over-density δ_l and potential ϕ_l , the short-wavelength modes of the density field are:

$$\delta_s = \alpha [(1 + 2f_{\text{NL}}\phi_l)\phi_s + f_{\text{NL}}\phi_s^2]. \quad (9)$$

This is a special case of

$$\delta_s = \alpha [X_1\phi_s + X_2\phi_s^2], \quad (10)$$

where $X_1 = 1 + 2f_{\text{NL}}\phi_l$ and $X_2 = f_{\text{NL}}$.

In the non-Gaussian case, the local number density of haloes of mass M is a function of not just δ_l , but also X_1 and X_2 : $n[\delta_l, X_1, X_2; P_s(k_s); M]$. The halo bias is then

$$b_L(M, k) = \bar{n}^{-1} \left[\frac{\partial n}{\partial \delta_l(\mathbf{x})} + 2f_{\text{NL}} \frac{d\phi_l(k)}{d\delta_l(k)} \frac{\partial n}{\partial X_1} \right], \quad (11)$$

where the derivative is taken at the mean value $X_1 = 1$. (There is no X_2 term since X_2 is not spatially variable.) The first term here is the usual Gaussian bias, which has no dependence on k .

Equation (10) shows that the effect on non-Gaussianity is a local rescaling of amplitude of (small scale) matter fluctuations. To keep the cosmologist's intuition we write this in terms of σ_8 :

$$\sigma_8^{\text{local}}(\mathbf{x}) = \sigma_8 X_1(\mathbf{x}), \quad (12)$$

so $\delta\sigma_8^{\text{local}} = \sigma_8 \delta X_1$. This allows us to rewrite Equation (11) as

$$b_L(M, k) = b_L^{\text{Gaussian}}(M) + 2f_{\text{NL}} \frac{d\phi_l(k)}{d\delta_l(k)} \frac{\partial \ln n}{\partial \ln \sigma_8^{\text{local}}}. \quad (13)$$

In principle there is an additional change in the bias because the mean density \bar{n} contains terms of order f_{NL} , which arise from (i) the dependence of n on X_2 and (ii) the cross-correlation of δ_l and X_1 . This correction is scale-independent and so cause no problem if one is fitting the bias to large-scale structure data, as we do here.

Substituting in $d\phi_l(k)/d\delta_l(k) = \alpha^{-1}(k)$ and dropping the *local* label, we find:

$$\Delta b(M, k) = \frac{3\Omega_m H_0^2}{c^2 k^2 T(k) D(z)} f_{\text{NL}} \frac{\partial \ln n}{\partial \ln \sigma_8}. \quad (14)$$

This formula is extremely useful because it applies to the bias of any type of object and is expressible entirely in terms of quantities in Gaussian cosmologies, which have received enormous attention from N -body simulators. Within the peak-background split model, the task of performing non-Gaussian calculations is thus reduced to an ensemble of Gaussian simulations with varying amplitude of matter fluctuations.

B. Application to universal mass functions

We now apply Equation (14) to halo abundance models with a universal mass function. Universal mass functions are those that depend only on significance $\nu(M)$, i.e.

$$n(M) = n(M, \nu) = M^{-2} \nu f(\nu) \frac{d \ln \nu}{d \ln M}, \quad (15)$$

where we define $\nu = \delta_c^2 / \sigma^2(M)$ and $f(\nu)$ is the fraction of mass that collapses into haloes of significance between ν and $\nu + d\nu$. Here $\delta_c = 1.686$ denotes the spherical collapse linear over-density and $\sigma(M)$ is the variance of the density field smoothed with a top-hat filter on the scale enclosing mass M . Universality of the halo mass function has been tested in numerous simulations, with results generally confirming the assumption even if the specific functional forms for $f(\nu)$ may differ from one another.

The significance of a halo of mass M depends on the background density field δ_l , so one can compute $\partial n / \partial \delta_l(\mathbf{x})$ and insert it into Equation (4) [51],

$$b = 1 - \frac{2}{\delta_c} \nu \frac{d}{d\nu} \ln[\nu f(\nu)]. \quad (16)$$

(This is > 1 for massive haloes since the last derivative is negative in this case.)

The derivative $\partial \ln n / \partial \ln \sigma_8$ appearing in Equation (14) can be obtained under the same universality assumption. In fact, the calculation is simpler. The definition of the significance implies $\nu \propto \sigma_8^{-2}$, so that $d \ln \nu / d \ln M$ does not depend on σ_8 at fixed M . Therefore $n \propto \nu f(\nu)$ and

$$\frac{\partial \ln n}{\partial \ln \sigma_8} = \frac{\partial \ln \nu}{\partial \ln \sigma_8} \frac{\partial \ln[\nu f(\nu)]}{\partial \ln \nu} = -2\nu \frac{d}{d\nu} \ln[\nu f(\nu)]. \quad (17)$$

Thus by comparison to Equation (16), we find:

$$\Delta b(M, k) = 3 f_{\text{NL}} (b - 1) \delta_c \frac{\Omega_m}{k^2 T(k) D(z)} \left(\frac{H_0}{c} \right)^2 \quad (18)$$

This is equivalent to the previously derived expressions [47, 52]. However, it is more general, because it is independent of the form of $f(\nu)$. It is therefore valid for the Press-Schechter mass function as well as for the more accurate Sheth-Tormen function. It is also valid for any object that obeys a halo occupation distribution (HOD) that depends only on the halo mass, $\langle N \rangle(M)$, since in this case both b and Δb are linearly averages of their values for individual masses:

$$b = \frac{\int b(M) n(M) \langle N \rangle(M) dM}{\int n(M) \langle N \rangle(M) dM}, \quad (19)$$

and similarly for Δb .

C. Halo merger bias

The above statements apply to biasing of objects whose HOD depends only on the mass of the halo. However this may not be true for the quasars; in particular there are many lines of evidence that suggests that quasar activity is triggered by recent mergers [53, 54, 55]. Therefore we should consider the standard bias b and large-scale bias Δb for recent mergers, which is in general not the same as the bias of all haloes of the final mass [56, 57].

This section considers the simplified case in which quasars are triggered by a merger between a halo of mass M_1 and one of mass M_2 , after which the quasar lives for a time $t_Q \ll H^{-1}$ in the new halo of mass $M_0 = M_1 + M_2$. This requires us to understand the dependence of the number of recent mergers on amplitude, which we will again express as σ_8 . Unlike the case of the mass function there are no accurate fitting formulae to the merger rate that have been tested against N -body simulations for a variety of cosmologies. Therefore we will take two approaches here. The first will be to consider the recent merger probabilities from the extended Press-Schechter (ePS) formalism. With ePS, we will find that for haloes of a given mass the probability of being a recent merger is proportional to σ_8^{-1} . In this picture, the bias of the quasars in this case is the same as the halo bias $b(M_0)$, but the f_{NL} -induced bias Δb is less for recent mergers than for all haloes of mass M_0 . However there is no rigorous error bound on ePS calculations, so it is desirable to have an independent way to get the dependence of merger histories on σ_8 . We therefore consider a second method of getting the recent merger probability during the matter-dominated era by using redshift scaling relations from N -body simulation results. The latter method confirms the ePS σ_8^{-1} relation.

1. Extended Press-Schechter calculation

We will work in the ePS formalism in which the merger history seen by a given dark matter particle is controlled by the linear density field $\delta(M)$ measured today, spherically smoothed on a mass scale M in Lagrangian space [58]. At time t a particle is inside a halo of mass $\geq M$ if $\delta(M') > \omega(t)$ for any $M' > M$, where $\omega(t) = \delta_c D(t_0) / D(t)$ is the ratio of the threshold over-density for collapse δ_c to the growth function $D(t)$. In this picture it is convenient to replace the smoothing scale M with the variance of the density field on that scale, $S(M) = \langle \delta(M)^2 \rangle$. The smoothed density field $\delta(S)$ then follows a random walk as a function of S ; this random walk is usually assumed to be Markovian because (i) each Fourier mode is independent for Gaussian initial conditions, and (ii) one neglects the difference between smoothing with a top-hat in Fourier space (in which each mode is independent) and the physically motivated top-hat in real space.

In this formalism we would like the probability that a

halo of mass M_0 at time t was actually of mass M_1 at an earlier time $t-t_Q$ and experienced a merger with a halo of mass $M_2 = M_0 - M_1$. As argued by Lacey & Cole [58], the probability for a particular dark matter particle in this halo to have been in an object of mass $< M_1$ at time $t-t_Q$ is the probability that the trajectory $\delta(S)$ does not exceed $\omega(t-t_Q)$ between $S_0 \equiv S(M_0)$ and $S_1 = S(M_1)$. This evaluates to

$$P_{\text{particle}}(< M_1) = \text{erfc} \frac{\omega(t-t_Q) - \omega(t)}{\sqrt{2(S_1 - S_0)}}, \quad (20)$$

so the differential probability is:

$$\begin{aligned} P_{\text{particle}}(M_1) dM_1 &= \frac{1}{\sqrt{2\pi}} \frac{\omega(t-t_Q) - \omega(t)}{(S_1 - S_0)^{3/2}} \\ &\times \exp \left\{ -\frac{[\omega(t-t_Q) - \omega(t)]^2}{2(S_1 - S_0)} \right\} \\ &\times \left| \frac{dS_1}{dM_1} \right| dM_1 \\ &\approx \frac{1}{\sqrt{2\pi}} \frac{t_Q |\dot{\omega}|}{(S_1 - S_0)^{3/2}} \left| \frac{dS_1}{dM_1} \right| dM_1, \end{aligned} \quad (21)$$

where in the last line we have assumed that t_Q is short so that one can do a Taylor expansion to lowest order in t_Q and recalled that $\dot{\omega} < 0$. The differential probability that the halo of mass M_0 is a recent merger is simply this divided by the fraction of the particles in the mass M_1 progenitor,

$$P(M_1|M_0) dM_1 = \frac{1}{\sqrt{2\pi}} \frac{t_Q |\dot{\omega}|}{(S_1 - S_0)^{3/2}} \frac{M_0}{M_1} \left| \frac{dS_1}{dM_1} \right| dM_1. \quad (22)$$

This formula was first derived by Lacey & Cole [58], albeit in a slightly different form [they computed $P(M_0|M_1)$]. It has two well-known deficiencies. One is that it is not symmetric under exchange of M_1 and M_2 , especially for extreme mass ratios [59, 60]. Another is that it does not contain merger bias in the Gaussian case, i.e. the bias of mergers is simply $b(M_0)$ [56]. This is because of the assumption that the trajectory $\delta(S)$ is a Markovian random walk, which is not quite correct. For example, the analytic explanations for merger bias of high-mass haloes [61] are based on non-Markovian behaviour due to the fact that the physically meaningful smoothing in real space does not correspond to a sharp cutoff at some k_{max} . The corresponding merger history bias is based on the correlation coefficient γ between $\delta(S)$ and $d\delta(S)/dS$; one would have $\gamma = 0$ if one used the Fourier-space rather than real-space top-hat filter. This subtlety is however not required to understand why the merger bias in f_{NL} cosmologies is significant on large scales.

For our application we would also need to integrate over the range of masses M_1 that define a major merger, but since the result does not actually depend on this we will not explicitly write it. In order to apply Equation

(14) to recent mergers we need only understand how the number density of recent mergers varies with σ_8 . Since the number density of recent mergers is the product of the number density of haloes of mass M_0 and the probability of them being recent mergers, we may write

$$\frac{\partial \ln n_{\text{merger}}}{\partial \ln \sigma_8} = \frac{\partial \ln n(M_0)}{\partial \ln \sigma_8} + \frac{\partial \ln P(M_1|M_0)}{\partial \ln \sigma_8}. \quad (23)$$

From Equations (16) and (17), the first term evaluates to $\delta_c(b-1)$. The second term contains the merger tree-dependent contribution to the large-scale bias, and can be evaluated from Equation (22). If one varies σ_8 , the mass variances all scale as $S(M) \propto \sigma_8^2$, and hence $P(M_1|M_0) \propto \sigma_8^{-1}$. Thus we conclude that the second term is equal to -1 , so

$$\frac{\partial \ln n_{\text{merger}}}{\partial \ln \sigma_8} = \delta_c(b-1 - \delta_c^{-1}). \quad (24)$$

This is identical to the extra large-scale bias for haloes of fixed mass, except that we have a factor of $b-1 - \delta_c^{-1}$ instead of $b-1$, so the factor of $b-1$ is replaced by $b-1.6$.

This formula is derived from ePS formalism and so it would seem to be on a somewhat less certain footing, since the analytic formulas for merger rates have not been tested in N -body simulations as extensively as those for the halo mass function. However, as we show in the following subsection, we do have some guidance from numerical simulations suggesting the scaling derived here is correct.

2. Scaling from N -body simulations

The ePS formalism predicts that the probability of a halo of mass M_0 being a recent merger, $P(M_1|M_0)dM_1$, is proportional to σ_8^{-1} . While the qualitative result that massive haloes are more likely to be recent mergers in low- σ_8 than high- σ_8 cosmologies is supported by N -body simulations [62, 63], the quantitative validity of the -1 exponent does not appear to be well-tested. Nevertheless, in the matter-dominated era it is possible to determine the exponent from the redshift dependence of the merger rate.

The key is that there is no preferred timescale in the Einstein-de Sitter cosmology; scale factor and linear growth factor are both proportional to $t^{2/3}$ and therefore the rescaling of initial amplitude is mathematically identical to rescaling of time. Hence two N -body simulations whose initial conditions differ only by the normalization of the primordial perturbations will evolve through exactly the same sequence of halo formation and mergers, except that the scale factor of each merger is re-scaled according to $a_{\text{merger}} \propto \sigma_8^{-1}$.

Note that for Λ CDM cosmologies this correspondence between scaling time and scaling normalisation breaks as the amplitude of fluctuations at the onset of cosmic acceleration will be different for different initial amplitudes.

Therefore results of this rescaling do not apply to the lowest redshifts, where the dark energy becomes important, but since in our analysis the only sample where recent mergers may be relevant is the quasar sample, which has a redshift distribution peaking at $z \sim 1.7$, this is a minor deficiency.

We want to test this relation from the merger history statistics [64] in the Millenium Simulation [65]. The recent merger probability, which we have denoted $P(M_1|M_0)dM_1$, is related to the merger rate B/n defined by Ref. [64] by:

$$P(M_1|M_0)dM_1 = t_Q \frac{B(M_0, \xi)}{n(M_0)} \frac{dz}{dt} \frac{\partial M_1}{\partial \xi} d\xi, \quad (25)$$

where $\xi > 1$ is the mass ratio of the progenitors. Here B/n is the merger rate per final halo of mass M_0 per unit redshift per unit ξ . The derivative with respect to σ_8 is straightforward to express:

$$\frac{\partial \ln P(M_1|M_0)}{\partial \ln \sigma_8} = \frac{\partial \ln(B/n)}{\partial \ln \sigma_8}, \quad (26)$$

where the partial derivatives are all at constant z .

In an Einstein-de Sitter universe, the rescaling of the amplitude

$$\sigma_8 \rightarrow (1 + \epsilon)\sigma_8 \quad (27)$$

is equivalent to rescaling of the scale factor (or redshift):

$$1 + z \rightarrow \frac{1 + z}{1 + \epsilon}. \quad (28)$$

Equating the recent merger probabilities in these two cases gives

$$\frac{B}{n} (1 + z, \sigma_8(1 + \epsilon)) dz = \frac{B}{n} \left(\frac{1 + z}{1 + \epsilon}, \sigma_8 \right) \frac{dz}{1 + \epsilon}. \quad (29)$$

[The denominator $1 + \epsilon$ on the right-hand side comes from rescaling of the redshift interval, $dz \rightarrow dz/(1 + \epsilon)$.] Taking the logarithm of both sides, and then differentiating with respect to ϵ gives

$$\frac{\partial \ln(B/n)}{\partial \ln \sigma_8} = -1 - \frac{\partial \ln(B/n)}{\partial \ln(1 + z)}. \quad (30)$$

This means that Equation (26) can be evaluated provided the power-law exponent relating B/n to $1 + z$ is known.

The ePS prediction is $B/n \propto (1 + z)^0$, i.e. constant [64]. Inspection of Figure 8 of Ref. [64] shows that for a wide range of halo masses ($\geq 2 \times 10^{12} M_\odot$) and progenitor mass ratios (100:1 through 3:1), the exponent is indeed close to 0 during the matter-dominated era $z > 1$, although in some cases (galaxy mass haloes, 3:1 mergers) the actual scaling is closer to $B/n \propto (1 + z)^{0.1}$. These results suggest the scaling $\partial \ln P(M_1|M_0)/\partial \ln \sigma_8$ is in the range of -1 (the ePS prediction) to -1.1 . If we plug this into Equation (23) then one derives $\partial \ln n_{\text{merger}}/\partial \ln \sigma_8$ equal to $\delta_c(b - 1.6)$ (for -1) or $\delta_c(b - 1.65)$ (for -1.1).

These results provide an independent calculation of $\partial \ln P(M_1|M_0)/\partial \ln \sigma_8$ that is on a more solid footing than ePS. The agreement of the logarithmic derivatives at the $\sim 10\%$ level is remarkable, especially given that ePS does not do so well at predicting the absolute merger rate.

3. Summary

We can write a generalised expression for the f_{NL} induced scale dependent bias as

$$\Delta b(M, k) = 3f_{\text{NL}}(b - p)\delta_c \frac{\Omega_m}{k^2 T(k) D(z)} \left(\frac{H_0}{c} \right)^2, \quad (31)$$

where $1 < p < 1.6$, i.e. $p = 1$ for objects populating a fair sample of all the halos in a given mass range and $p = 1 + \delta_c^{-1} \sim 1.6$ for objects that populate only recently merged halos. Below we discuss plausible values of p for the data samples used in this paper.

To summarize, in non-Gaussian cosmologies, there are two types of merger bias: both b and Δb can depend on the merger history of a halo as well as its final mass. The ePS prediction for recent mergers is that for the bias $b = b(M_0)$, i.e. there is no dependence on merger history; but that recent mergers with final mass M_0 have a smaller Δb than one would find considering all haloes of mass M_0 . Under the specific assumptions of ePS, if one makes the extreme assumption that all quasars are the result of recent halo mergers, the correction can be implemented by replacing $b - 1$ in Equation (18) with $b - 1.6$.

The reliability of the ePS result can only be evaluated by comparison to N -body simulations. In the matter dominated era, in the range of masses and progenitor mass ratios covered by Ref. [64], ePS appears to be a good description for the merger bias of Δb .

Since in practice one estimates Δb from the observed clustering rather than from the unobserved halo mass M_0 , any assembly bias effects in b [66] are also important to our analysis. This subject has received much attention recently, with the general result being that for high-mass haloes ($M \gg M_*$), those haloes that exhibit substructure, have lower concentration, or are younger have a slightly higher bias than the mean $b(M)$. For example, in [67] it was found that the lowest quartile of haloes in concentration has bias ~ 10 – 20% higher than the mean $b(M)$. Ref. [68] found that the lowest-concentration quintile was $\sim 10\%$ more biased than their highest-concentration quintile, and that this dependence was even weaker if one split on formation redshift instead of concentration. Ref. [69] found almost no dependence on formation redshift in the relevant range $\delta_c/\sigma \geq 2$, but their lowest quintile of concentration is $\sim 25\%$ more biased than the mean $b(M)$ and even larger effects are seen if one splits by substructure. Ref. [57] found that the bias for recent major mergers was enhanced by $\sim 5\%$ relative

to $b(M)$. It is clear that the strength of this effect depends strongly on the second parameter used, but in the case of the definitions related to the mergers, the deviation in $b(M)$ is significantly less than the corrections to the Δb , which replaces $b - 1$ with $b - 1.6$. We will therefore assume that the theoretical uncertainties are fully absorbed by the expression in Equation (31).

Finally, while there is ample evidence that quasar activity is often triggered by mergers, it is probably not the case that all quasars live in recently merged halos. Therefore the true value of p for quasar population lies between 1 and 1.6, since the true population of host halos lies somewhere between randomly selected halos and recently merged halos. Therefore, our limits with $p \sim 1.6$ should be viewed as a most conservative reasonable option.

III. METHOD AND DATA

After reviewing and extending the theoretical formalism we turn to its application to the real data. We would like to use Equation (31) to put constraints on the value of the f_{NL} parameter. Since the effect is significant only on very large scales we need to use the tracers of large scale structure at the largest scales available. In addition, the effect scales as $b - p$, where p is typically 1 but can be as large as 1.6 in special cases, hence we need very biased tracers of large scale structure to measure the effect. We discuss below our choice of observational data. Finally, the effect changes the power on large scales and in principle this can also be achieved with a change in the primordial power spectrum, although this degeneracy exists only in the presence of one tracer: with two tracers with different biases one can separate f_{NL} from the changes in the initial power spectrum. Here we assume that the basic model is one predicted by the simplest models of structure formation and we do not allow for sudden changes in the power spectrum beyond what is allowed by the standard models, which assume the power spectrum slope n_s to be constant. We use Markov Chain Monte Carlo method to sample the available parameter space using a modified version of the popular public package `cosmomc` [70]. In addition to f_{NL} , we fit for the standard parameters of the minimal concordance cosmological model: $\omega_b = \Omega_b h^2$, $\omega_{\text{CDM}} = \Omega_{\text{CDM}} h^2$, θ , τ , n_s and $\log A$, where θ is the ratio of the sound horizon to the angular diameter distance at decoupling (acting as a proxy for Hubble's constant), τ is the optical depth and A is the primordial amplitude of the power spectrum. All priors are wide enough so that they do not cut the posterior at any plane in the parameter space.

We always use standard cosmological data as our baseline model. These include the WMAP 5-year power-spectra [71, 72] and additional smaller-scale experiments (VSA, CBI, ACBAR) [73, 74, 75], as well as the supernovae measurements of luminosity distance from the Supernova Legacy Survey (SNLS) [76]. For values of f_{NL}

under consideration in this paper these data sets are not directly sensitive to the f_{NL} parameter. However, they are needed to constrain the basic cosmological model and thus the shape and normalisation of the matter power spectrum. The large scale structure data discussed below are thus simultaneously able to fit for f_{NL} and other auxiliary parameters.

Most of our large-scale structure data is drawn from the Sloan Digital Sky Survey (SDSS). The SDSS drift-scans the sky in five bands (*ugriz*) [77] under photometric conditions [78, 79] using a 2.5-meter optical telescope [80] with 3 degree field of view camera [81] located in New Mexico, USA [78]. The photometric and astrometric calibration of the SDSS and the quality assessment pipeline are described by Refs. [82, 83, 84, 85, 86]. Bright galaxies [87], luminous red galaxies (LRGs) [88], and quasar candidates [89] are selected from the SDSS imaging data for spectroscopic follow-up [90]. This paper uses imaging data through the summer of 2005, which was part of SDSS Data Release 6 (DR6) [91], and spectroscopic data through June 2004 (DR4) [92].

The requirement of large scales and highly biased tracers leads us to explore several different large scale data sets, in particular SDSS LRGs, both spectroscopic [93] and photometric [94] samples, and photometric quasars (QSOs) from SDSS [95]. In all these cases we use auto-correlation power spectrum, which is sensitive to f_{NL}^2 . These datasets can be assumed to be statistically independent. As explained below, when spectroscopic and photometric LRGs are analysed together, we take care to exclude those photometric redshift bins that have significant overlap with spectroscopic sample. Our quasars have typical redshifts of $z \sim 1.5 - 2$ and only 5% overlap with LRGs due to photoz errors. Moreover, they are in the Poisson noise limited regime, so overlap in volume is less relevant. This is discussed in more detail in [95]. In addition, we also use cross-correlation of all these samples, as well as nearby galaxies from the 2-micron All-Sky Survey (2MASS) [37] and radio sources from the NRAO VLA Sky Survey (NVSS) [96] with CMB, as analyzed in Ho et al. [95]. Since this is a cross-correlation between the galaxies and matter (as traced by the ISW effect), the dependence is linear in f_{NL} .

A. Spectroscopic LRGs from SDSS

We use the spectroscopic LRG power spectrum from Tegmark et al. [93], based on a galaxy sample that covers 4000 square degrees of sky over the redshift range $0.16 \leq z \leq 0.47$. We include only bins with $k \leq 0.2h/\text{Mpc}$. We model the observed data as

$$P_{\text{observed}}(k) = [b + \Delta b(k, f_{\text{NL}})]^2 P_{\text{lin}}(k) \frac{1 + Qk^2}{1 + Ak}, \quad (32)$$

where the last term describes small-scale non-linearities [97], with Q treated here as a free parameter (bound between zero and 40) and $A = 1.4h^{-1} \text{ Mpc}$. For realistic

values of f_{NL} and Q , the non-Gaussian bias Δb is present only at large scales and the Q -term is present only at small scales; there is no range of scales over which both are important. We explicitly confirmed that there is no correlation between Q and f_{NL} present in our MCMC chains and we let the data to determine the two parameters.

As discussed above if the halos in which objects reside have undergone recent mergers and thus depend on properties other than halo mass then the simple scaling with $(b-1)$ may not be valid. This is unlikely to be relevant for LRGs, which are old red galaxies sitting at the center of group and cluster sized halos. Moreover, number density of LRGs is so high that it is reasonable to assume that almost every group sized halo contains one, since otherwise it is difficult to satisfy both the number density and high bias at the same time [98]. For LRGs we thus do not expect there is a second variable in addition to halo mass and halo occupation models find that populating all halos with mass above $10^{13} M_{\odot}/h$ with an LRG is consistent with all the available data [99]. Hence we will only use $p = 1$ in Equation (31). The same also holds for the photometric LRGs discussed below.

B. Photometric LRGs from SDSS

We use data from Padmanabhan et al. [94], who provide the LRG angular power spectrum measured in 8 redshift slices (denoted 0–7) covering the range $0.2 < z_{\text{photo}} < 0.6$ in slices of width $\Delta z_{\text{photo}} = 0.05$. The power spectrum is based on 3500 square degrees of data. We use only data-points that correspond to $k < 0.1h/\text{Mpc}$ at the mean redshift of each individual slice. We use the full Bessel integration to calculate the angular power spectrum on largest scales and account for the redshift-distortion power as described in Padmanabhan et al. [94]:

$$C_{\ell} = C_{\ell}^{gg} + C_{\ell}^{gv} + C_{\ell}^{vv}, \quad (33)$$

where superscripts g and v denote galaxies over-density and velocity terms respectively. The bias and β dependence has been put back into the Bessel integral as it now depends on the value of k . The three terms are given by the integrals:

$$\begin{aligned} C_{\ell}^{gg} &= 4\pi \int \frac{dk}{k} \Delta^2(k) |W_{\ell}(k)|^2, \\ C_{\ell}^{gv} &= 8\pi \int \frac{dk}{k} \Delta^2(k) \Re [W_{\ell}^*(k) W_{\ell}^r(k)], \quad \text{and} \\ C_{\ell}^{vv} &= 4\pi \int \frac{dk}{k} \Delta^2(k) |W_{\ell}^r(k)|^2, \end{aligned} \quad (34)$$

where $\Delta^2(k)$ is the linear matter power spectrum today. The window functions are given by

$$\begin{aligned} W_{\ell}(k) &= \int (b + \Delta b) \frac{D(r)}{D(0)} \frac{dN}{dr} j_{\ell}(kr) dr \quad \text{and} \\ W_{\ell}^r(k) &= \int \Omega_m^{0.6}(r) \frac{D(r)}{D(0)} \frac{dN}{dr} \left[\frac{2\ell^2 + 2\ell - 1}{(2\ell - 1)(2\ell + 3)} j_{\ell}(kr) \right. \\ &\quad \left. - \frac{\ell(\ell - 1)}{(2\ell - 1)(2\ell + 1)} j_{\ell-2}(kr) \right. \\ &\quad \left. - \frac{(\ell + 1)(\ell + 2)}{(2\ell + 1)(2\ell + 3)} j_{\ell+2}(kr) \right] dr, \end{aligned} \quad (35)$$

where dN/dr is the redshift distribution normalised to unity and written in terms of comoving distance r , and D is the growth function. The code automatically switches to the Limber approximation when this becomes accurate. Note that for the low multipoles, it is essential to include the redshift-space distortion even for a photometric survey because a significant amount of power comes from Fourier modes that are not transverse to the line of sight.

We use an independent bias parameter for each redshift slice. In addition to the bias dependence, we also use the Equation (32) to take into account non-linear corrections. While strictly speaking the value of Q should be different for each slice, we use a single free parameter Q for all slices. We have explicitly checked that non-linear corrections are negligible for $k < 0.1h/\text{Mpc}$ and therefore this is not a major issue. Since there is a strong overlap between the spectroscopic and photometric sample for $z < 0.45$, we use only slices 5–7 when combining this data with spectroscopic sample.

C. Photometric quasars from SDSS

We use the power spectrum of the high redshift quasar photometric sample that has recently been constructed for ISW and CMB lensing cross-correlation studies [95, 100]. The sample covers 5800 square degrees of sky and originally had two photometric redshift ranges, $0.65 < z_{\text{photo}} < 1.45$ (“QSO0”) and $1.45 < z_{\text{photo}} < 2.00$ (“QSO1”). It consists of ultraviolet-excess (UVX; $u - g < 1.0$) point sources, classified photometrically as quasars [101], and with photometric redshifts [102]. The classification and photometric redshifts were at the time of sample construction only available over a subset of the survey region; they were extended to the remaining region using a nearest-neighbor algorithm in color space [95]. As described below, we only used the QSO1 sample as QSO0 appears to suffer from systematic errors on large scales.

The largest angular scales in the quasar data are subject to at least three major sources of systematic error: stellar contamination, errors in the Galactic extinction maps, and calibration errors. All of these are potentially much worse than for the LRGs: some stars (e.g. M dwarf-white dwarf binaries) can masquerade as quasars, and we

are relying on the u band where extinction is most severe and the photometric calibration is least well understood. These errors were discussed in the context of ISW studies [95], but if one wishes to use the quasar auto-power spectrum on the largest angular scales the situation is more severe.

We investigated this subject by computing the cross-power spectrum of each QSO sample with the SDSS $18.0 < r < 18.5$ star sample and with “red” stars (which satisfy the additional cut $g - r > 1.4$). The cross-power should be zero in the absence of systematics but it could be positive if there is stellar contamination in the QSO sample. Either positive or negative correlation could result from photometric calibration errors which shift the quasar and stellar locus in nontrivial ways. The results of this correlation are shown in Figure 1, with error bars estimated from the usual harmonic space method,

$$\sigma(C_\ell^{qs}) = \frac{\sqrt{(C_\ell^{qq} + n_q^{-1})C_\ell^{ss}}}{[(\ell_{\max} + 1)^2 - \ell_{\min}^2]f_{\text{sky}}}, \quad (36)$$

where C_ℓ^{qq} is the quasar autopower spectrum, n_q is the number of quasars per steradian, and C_ℓ^{ss} is the star autopower spectrum; the n_s^{-1} term is negligible. (Aside from boundary effects, this is the same error that one would obtain by correlating random realizations of the quasar field with the actual star field.) From the figure, QSO1 appears clean, but QSO0 appears contaminated: the first bin ($2 \leq \ell < 12$) has a correlation of $C_\ell^{qs} = -(2.9 \pm 1.0) \times 10^{-4}$ with the red stars. This is a -2.9σ result and strongly suggests some type of systematic in the QSO0 signal on the largest angular scales. We are not sure of the source of this systematic, but the amount of power in the quasar map that is correlated with the red stars is

$$\frac{\ell(\ell+1)}{2\pi}C_\ell^{qq}(\text{corr}) = \frac{\ell(\ell+1)}{2\pi}\frac{C_\ell^{qs2}}{C_\ell^{ss}} \sim 2 \times 10^{-4}. \quad (37)$$

The variation in QSO0 density that is correlated with the red stars is thus at the $\sim 1.4\%$ level. This is consistent with the excess auto-power in QSO0 in the largest scale bin, which is at the level of $[\ell(\ell+1)/2\pi]C_\ell^{qq} \sim 3 \times 10^{-4}$ (see figure 10 in [95]) and is comparable to what one might expect from the 1–2% calibration errors in SDSS [84], although other explanations such as the extinction map are also possible. Because of this evidence for systematics, we have not used the QSO0 autopower spectrum in our analysis; in what follows we only use QSO1. QSO0 may be added in a future analysis if our understanding of the systematics improves.

Because the redshift distribution is poorly known and needs to be determined internally from the data sample itself the data is analyzed in a two step procedure:

1. Power spectrum points with $\ell = 30 \dots 200$ are used to constrain the product $(bdn/dz)(z)$, where b is the linear bias at redshift z and dn/dz is the normalised radial window function. Although the f_{NL} is taken into account at this step, its effect is sub-dominant.

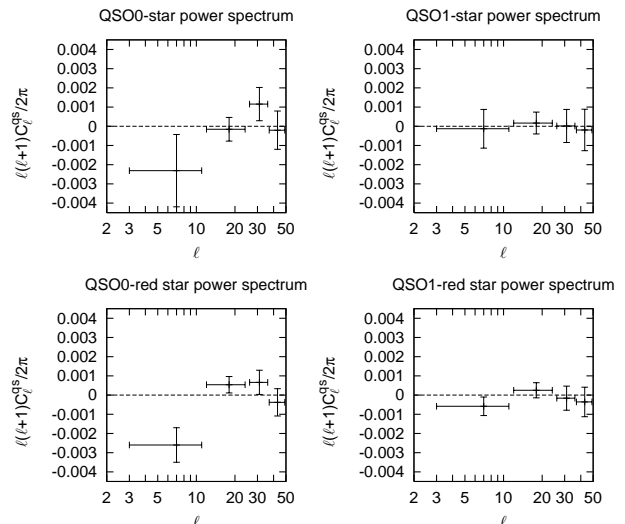


FIG. 1: The correlation of each quasar sample with stars and with the red stars.

2. We then assume that the functional form for $b(z)$ is either

$$b(z) \propto 1 + \left(\frac{1+z}{2.5}\right)^5 \quad (38)$$

as measured in [103], or that its form is given by

$$b(z) \propto 1/D(z), \quad (39)$$

as would be valid if the clustering amplitude is not changing with redshift. In both cases the constant of proportionality is determined from the normalisation condition

$$\int \frac{dn}{dz} dz = \int \frac{bdn}{dz} \frac{1}{b(z)} dz = 1. \quad (40)$$

3. Once both dn/dz and $b(z)$ are known we calculate the theoretical angular power spectrum using the same code as for photometric LRGs, taking into account all available ℓ points. This is the theoretical spectrum that is used to calculate the χ^2 that goes into the MCMC procedure. In principle, all free parameters that determine the shape of bdn/dz should be varied through the MCMC, rather than being fixed at the best-fit point. However, in the limit of Gaussian likelihood, the two procedures are equivalent, while the latter offers significant speed advantages.
4. We calculate χ^2 using two different methods. Our standard method is to use all points and the full covariance matrix assuming a Gaussian likelihood:

$$\chi^2 = (\mathbf{d} - \mathbf{t}) \cdot \mathbf{C}^{-1}(\mathbf{d} - \mathbf{t}), \quad (41)$$

where \mathbf{d} and \mathbf{t} are data and theory vectors of C_ℓ 's, respectively. This is likely to be a good approximation except on the largest scales, where small number of modes leads to corrections that may affect

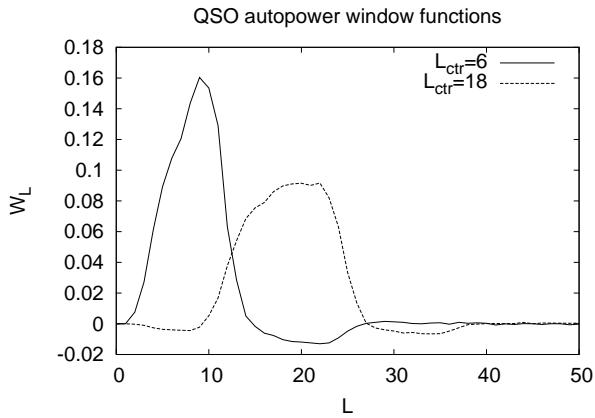


FIG. 2: The window functions for the $\ell = 6$ and $\ell = 18$ bins of the quasar power spectrum.

the outer limits (e.g. 3σ). To test this we model the first QSO bin with an inverse- χ^2 distribution, but neglecting covariance of this bin with higher ℓ bins:

$$\chi^2 = N \left[\ln \left(\frac{d_\ell + 1/n}{t_\ell + 1/n} \right) + \frac{t_\ell + 1/n}{d_\ell + 1/n} - 1 \right] + \text{Gaussian } \chi^2 \text{ for other points,} \quad (42)$$

where $N \sim 21.5$ is the effective number of modes contributing to the first bin and n is the number of quasars per steradian. (This was called the “equal variance” case in Ref. [104], and is appropriate if there is equal power in all modes; this is the case here to a first approximation since we find that the Poisson noise $1/n$ dominates.)

Since the power rises dramatically at low ℓ in the f_{NL} models, we have included the full window function in our calculation of the binned power spectrum, $C_{\text{bin}} = \sum_\ell W_\ell C_\ell$. The window functions for the lowest two QSO bins are shown in Figure 2, and the algorithm for their computation is presented in Appendix A.

As shown in the Section II C 1, if halos have undergone recent mergers then we would expect $p \sim 1.6$ instead of $p \sim 1$ in Equation (31). Recent mergers could be a plausible model for QSOs, whose activity could be triggered by a merger [53, 54, 55]. For QSOs used in this work we do not find that their number density places a significant constraint: at $z \sim 1.8$ the number density of halos with $b \sim 2.5 - 3$ is one to two orders of magnitude higher than the measured number density, hence we can easily pick and choose the halos with a recent merger and still satisfy the combined number density and bias constraint. This is in agreement with conclusions of [103], which looked at a similar QSO sample from 2dF. Because of this uncertainty we therefore run another separate analysis for QSOs with $p = 1.6$ (QSO merger case).

D. Cross-correlation between galaxies and dark matter via Integrated Sachs-Wolfe effect

One can also look for the f_{NL} using the cross-correlation between a tracer like galaxies or QSOs and dark matter. Since we do not have dark matter maps from large scales we can use cosmic microwave background (CMB) maps as a proxy. If the gravitational potential is time dependent, as is the case in a universe dominated by dark energy or curvature then this leads to a signature in CMB, the so-called integrated Sachs-Wolfe (ISW) effect [105]. This signature can easily be related to the dark matter distribution, but part of the signal is not coming from ISW but from the primary CMB anisotropies at the last scattering surface. These act as a noise and lead to a large sampling variance on large scales and as a result the statistical power of this technique is weakened. At the moment ISW is only detected at $\sim 4\sigma$ level [106]. Our procedure closely follows that of [95] and is in many respects very similar to that of the Section III C. We use all 9 samples present in Ho et al., although the discriminating power is mostly coming from the NVSS-CMB cross-correlation because NVSS sample is available over 27 361 deg^2 area and the tracers, radio galaxies, are biased with $b \sim 2$. First, bdn/dz and $b(z)$ are determined for each sample. Here we always use $b(z) \propto 1/D(z)$ for all samples except the quasar sample. Then we calculate the ISW Limber integral:

$$C_\ell^{gT} = \frac{3\Omega_m H_0^2 T_{\text{CMB}}}{c^3 (\ell + 1/2)^2} \int dz [b(z) + \Delta b(k(z), z)] \times \frac{dn}{dz} \frac{d}{dz} \left[\frac{D(z)}{D(0)} (1+z) \right] D(z) P(k(z)), \quad (43)$$

where $k(z) = (\ell + 1/2)/\chi$. Again, we used the full window function for the NVSS-CMB correlation to avoid an unnecessary bias and we assume $p = 1$ for all the samples.

IV. RESULTS

We begin by plotting data-points and theoretical predictions for six of the datasets and values of f_{NL} in Figure 3. This plot deserves some discussion. The easiest and most intuitive to understand is the case of spectroscopic LRGs. We note that the inclusion of the f_{NL} parameter modifies the behaviour of the power spectrum on the largest measured scales. Naively, one would expect LRGs to be very competitive at constraining f_{NL} . In practice, however, f_{NL} is degenerate with matter density, which also affects the shape of the power spectrum and hence the constraints are somewhat weaker. Since the effect of f_{NL} raises very strongly, just a couple of points on largest scales might break this degeneracy, improving constraints by a significant factor. The effect in the photometric LRG samples is similar, although we are now looking the angular space, where the dependence

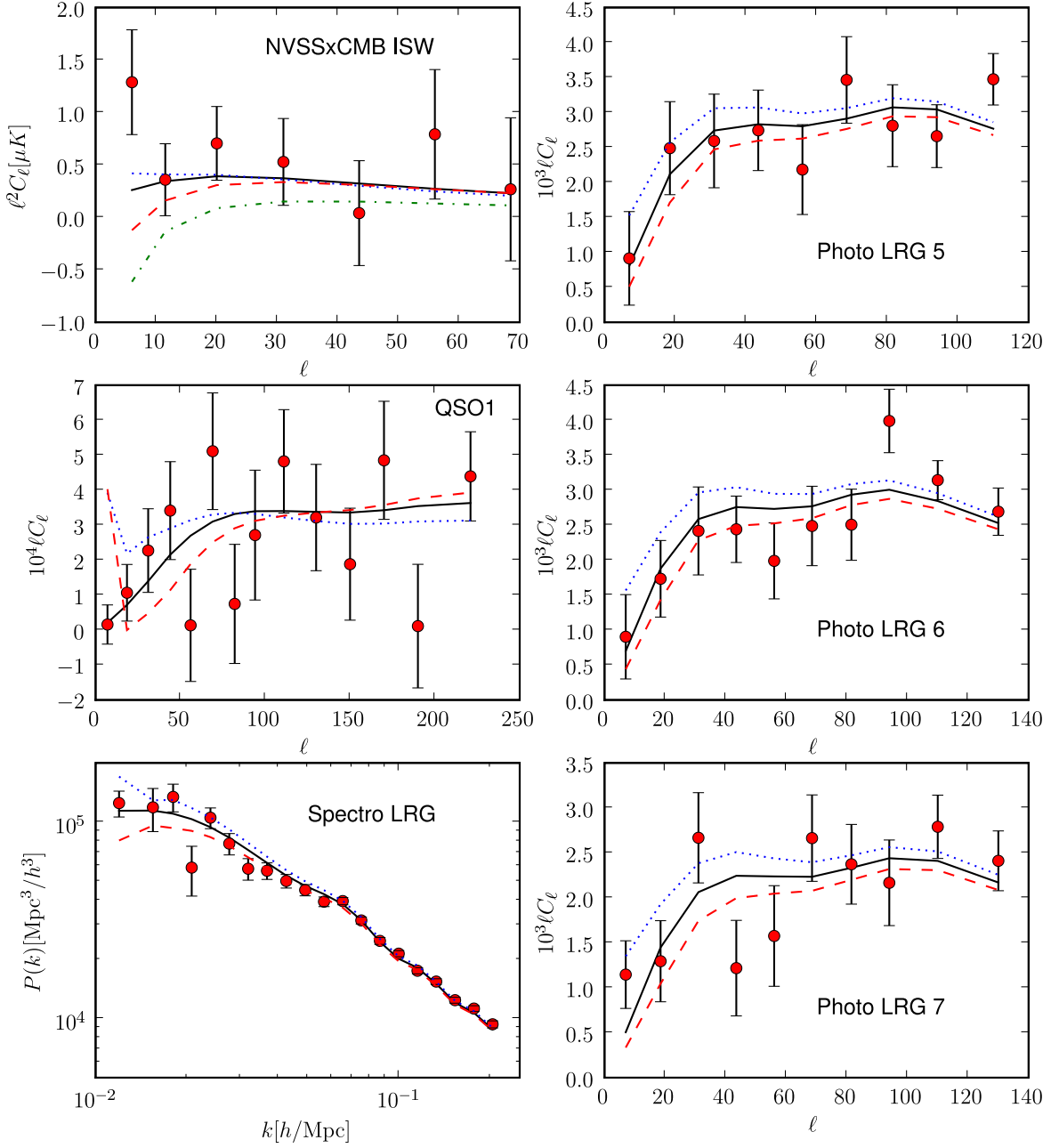


FIG. 3: This figure shows 6 datasets that are most relevant for our constraints on the value of f_{NL} . In the left column show the NVSSxSMB Integrate Sach Wolfe Cross correlation, the QSO1 power spectrum, the spectroscopic LRG power spectrum, while the right column shows the last three slices of the photometric LRG sample. The lines show the best fit $f_{\text{NL}} = 0$ model (black, solid) and two non-Gaussian models: $f_{\text{NL}} = 100$ (blue, dotted), $f_{\text{NL}} = -100$ (red, dashed). The ISW panel additionally shows the $f_{\text{NL}} = 800$ model as green, dot-dashed line. While changing f_{NL} , other cosmological parameters were kept fixed. See text for further discussion.

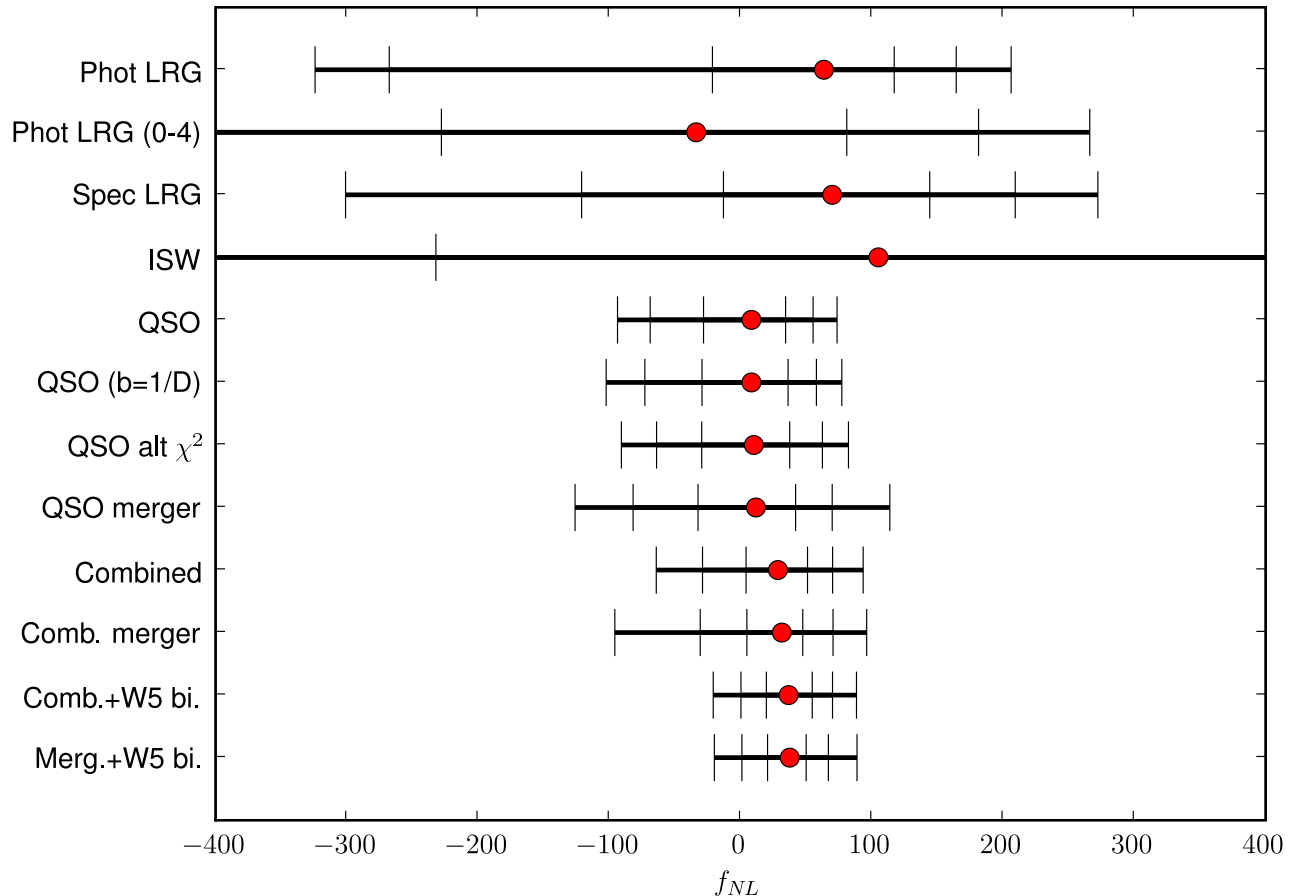


FIG. 4: This figure shows the median value (red points) and 1,2 and 3-sigma limits on f_{NL} obtained from different probes (vertical lines). The data set used are, from top to bottom: Photometric LRGs, Photometric LRGs with only slices 0–4 used, Spectroscopic LRGs, Integrated Sach Wolfe effect, photometric QSO, photometric QSOs using $b(z) \propto 1/D(z)$ biasing scheme (see Section III C), photometric QSOs using alternative χ^2 calculation scheme (see Section III C), using a scale dependent bias formula appropriate for recently merged halos (Section II C), Combined sample, Combined sample using a scale dependent bias formula appropriate for recently merged halos (for QSO), the last two results to which a statistically independent WMAP 5 bispectrum f_{NL} constraint was added. See text for discussion.

has been smeared out. The QSO plot again shows similar behaviour, with two caveats. First, the changes in the predicted power spectrum on small scales are a result of the fact that bdn/dz is perturbed with changing f_{NL} , although this is a minor effect. Second, the increase in the power at smallest ℓ for negative f_{NL} is due to the fact that for sufficiently negative f_{NL} (or sufficiently large scales), $\delta b < -2b$ and hence power spectrum rises again above what is expected in the Gaussian case. The more unexpected is the NVSS-CMB cross-correlation. Naively, one would expect that the first point of that plot will produce a very strong f_{NL} “detection”. However, the CMB cross-correlation signal is only linearly dependent on f_{NL} , while cross-correlations of NVSS with other tracers of structure are quadratically dependent on f_{NL} . Large values

of f_{NL} produce anomalously large power in the angular power spectrum if bdn/dz has significant contribution at high- z tail, which probes large scales. Therefore, the bdn/dz fitting procedure skews the distribution towards lower redshifts, leading to a lower bias overall. At very large values, e.g. $f_{NL} = 800$, this effect is so severe that the $b \propto 1/D(z)$ scaling forces $b < 1$ at the low-redshift end. This implies $\Delta b < 0$, and the large-scale ISW signal actually goes negative (see top-left panel of Fig. 3). Therefore, the ISW is surprisingly bad at discriminating f_{NL} and we were unable to fit the first NVSS ISW data point with a positive f_{NL} . This behavior is however only of academic interest because the other data sets strongly rule out these extreme values of f_{NL} .

We ran a series of MCMC chains with base cosmolog-

Data set	f_{NL}
Photometric LRG	$63^{+54+101+143}_{-85-331-388}$
Photometric LRG (0-4)	$-34^{+115+215+300}_{-194-375-444}$
Spectroscopic LRG	$70^{+74+139+202}_{-83-191-371}$
ISW	$105^{+647+755+933}_{-337-1157-1288}$
QSO	$8^{+26+47+65}_{-37-77-102}$
QSO (b=1/D)	$8^{+28+49+69}_{-38-81-111}$
QSO alternative χ^2	$10^{+27+52+72}_{-40-74-101}$
QSO merger	$12^{+30+58+102}_{-44-94-138}$
Combined	$28^{+23+42+65}_{-24-57-93}$
Comb. merger	$31^{+16+39+65}_{-27-62-127}$
Combined + WMAP5 bispectrum f_{NL}	$36^{+18+33+52}_{-17-36-57}$
Combined merger + WMAP5 bispectrum f_{NL}	$36^{+13+29+53}_{-17-36-57}$

TABLE I: Marginalised constraints on f_{NL} with mean, 1σ (68% c.l.), 2σ (95% c.l.) and 3σ (99.7%) errors. Ordering exactly matches that of the Figure 4. See text for discussion.

ical data and one of the four data sets considered above, as well as a run in which all data were combined (with the exception of slices 0–4 of photometric LRGs as described above). The results are summarized in Table I and visualized in the Figure 4.

We note several interesting observations. When only slices 0–4 of the photometric LRG sample are used, the results are weaker than those of the spectroscopic LRGs. The two trace comparable volume, but photometric sample does not use radial mode information and as a result its errors are expectedly larger. On the other hand, the overall photometric sample performs somewhat better than the spectroscopic LRG sample, due to its larger volume: it traces LRGs up to $z \sim 0.6$ as opposed to $z \sim 0.45$ for spectroscopic sample.

We find that the ISW is constraining the f_{NL} parameter rather weakly. This is somewhat disappointing, but not surprising, since the cross-correlation between LSS and CMB is weak and has only been detected at a few sigma overall. In addition, as mentioned above, f_{NL} enters only linearly (rather than quadratically) in the ISW expressions and is strongly degenerate with determination of bdn/dz . Given that ISW S/N can only be improved by another factor of ~ 2 at most even with perfect data we do not expect that it will ever provide competitive constraints on f_{NL} .

We find that the quasar power spectra give the strongest constraints on f_{NL} . This is due to their large volume and high bias. The lowest ℓ point in this data set at $\ell = 6$ is a non-detection and therefore highly con-

strains f_{NL} in both directions. The second and third point have some excess power relative to the best fit $f_{\text{NL}} = 0$ model and so give rise to a slightly positive value of f_{NL} in the final fits. This is however not a statistically significant deviation from $f_{\text{NL}} = 0$.

We also test the robustness of f_{NL} constraints from the quasar sample power spectrum by performing the following tests. First we replace the form of evolution of bias from that in Eq. (38) to that in Eq. (39). Second we replaced the details of the likelihood shape for the first points, we replace Eq. (41) with Eq. (42). In both cases, the effect on the constraints was minimal, as shown in the Figure 4 and the Table I.

The large-scale quasar power spectrum could also be affected by spurious power (e.g. calibration fluctuations or errors in the Galactic extinction map) or 1-halo shot noise, either of which would dominate at large scales over the conventional $P(k) \propto k$ autocorrelation. At the level of the current data these are not affecting our results: uncorrelated power adds to the power spectrum C_ℓ , and if present it would only tighten the upper limits on the power spectrum given by our $\ell = 6$ and 18 points. The 1-halo shot noise would contribute an added constant to C_ℓ since $z \sim 1.7$ haloes are unresolved across our entire range of ℓ ; the observed power at $\ell \sim 250$ constrains the 1-halo noise to be much less than the error bars at $\ell = 6, 18$. Nevertheless, if we had detected excess power in the quasars at the largest scales, a much more detailed analysis would have been necessary to show that it was in fact due to f_{NL} and not to systematics.

If quasars are triggered by mergers, then they do not reside in randomly picked halos and the use of the Eq. (18) may not be appropriate. As discussed in Section II C, one can replace the $(b - 1)$ factor in Eq. (18) with a modified factor $(b - 1.6)$. We quote the results in this case in the Table I as “QSO merger.” The error bars have increased by about 40%, which is somewhat less than naively expected from a population with an average bias of around 2.5. This is due to various feedback related to bdn/dz fitting. Moreover, this is likely to be an extreme case since it assumes that all quasars live in recently merged halos with short lifetimes, so we would expect that the true answer is somewhere in between the two results. On the other hand, it is also unclear how accurate extended Press-Schechter formalism is for this application, so there is some uncertainty associated with this procedure. Recent progress in understanding quasar formation and its relation to the underlying halo population [54] gives us hope that this can be solved in the future.

We also quote results for the combined analysis. In this case, the error on f_{NL} shrinks somewhat more than one would expect assuming that error on f_{NL} measurement from each individual dataset is independent. This is because other parameters, notably matter density and amplitude of fluctuations get better constrained when data are combined. Furthermore, we note that when quasars are assumed to be recent mergers the errors expand by

an expected amount at the 3σ level, but hardly at a 2σ level. We have carefully investigated this anomaly and it seems to be due a peculiar shape of the likelihood surface and subtle interplay of degeneracies between f_{NL} , matter density and amplitude of fluctuations.

V. DISCUSSION

The topic of this paper is signature of primordial non-Gaussianity of local type (the so called f_{NL} model) in the large scale structure of the universe. Specifically, it was recently shown that this type of non-Gaussianity gives rise to the scale dependence of the highly biased tracers [47]. We extend this analysis by presenting a new derivation of the effect that elucidates the underlying assumptions and shows that in its simplest form it is based on the universality of the halo mass function only. Our derivation also allows for possible extensions of the simplest model, in which tracers of large scale structure depend on properties other than the halo mass. One that we explore in some detail is the effect of recent mergers. By using extended Press-Schechter model we show that in this case the effect has the same functional form, but the predicted scaling with f_{NL} for a given bias has a smaller amplitude than in the simplest model.

Second, we apply these results to constrain the value of f_{NL} from the clustering of highly biased tracers of large scale structure at largest scales. In our analysis we find that the best tracers are highly biased photometric quasars from SDSS at redshifts between 1.5 and 2, followed by photometric and spectroscopic LRGs at redshift around 0.5. Our final limits at 95% (99.7%) confidence are

$$-29 (-65) < f_{\text{NL}} < +70 (+93) \quad (44)$$

if we assume halos in which tracers reside are a fair sample of all halos of a given bias. If we assume instead that QSOs are triggered by recent mergers and have short lifetimes then we find

$$-31 (-96) < f_{\text{NL}} < +70 (+96), \quad (45)$$

a somewhat weaker, but still competitive constraint. In both cases, we find no evidence for non-zero f_{NL} . These results shows that existing data can already put very strong limits on the value of f_{NL} , which are competitive with the best constraints from WMAP 5 year analysis of CMB bispectrum[5], which is statistically independent of the method used in this paper. These give $-9 < f_{\text{NL}} < 111$ at 95% confidence. Assuming that WMAP5 constraint on f_{NL} to independent of n_s and well described by a Gaussian likelihood $f_{\text{NL}} = 51 \pm 31$ [5], we get the following combined constraint:

$$0 (-21) < f_{\text{NL}} < +69 (+88). \quad (46)$$

If we assume quasars to live in recently merged halos, we get essentially the same result with the upper limit relaxed to 89.

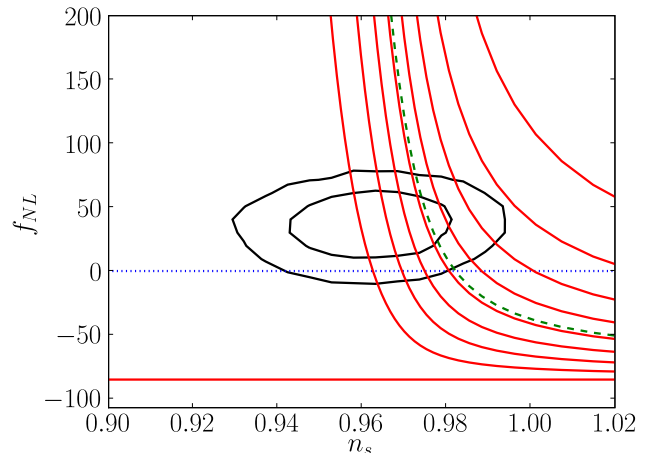


FIG. 5: This figure shows 1 and 2σ contours on the n_s - f_{NL} plane for our best combined data set with additional WMAP 5 year bispectrum constraint (assumed to be independent of n_s). Red lines are predictions from the ekpyrotic models and correspond to values of fixed γ and varying ϵ . Different line correspond to different values of γ , which varies between $\gamma = -1$ (flat, constant, negative f_{NL}) to $\gamma = -0.2$ in steps of 0.1. The dashed green line corresponds to the theoretically favored value of $\gamma = -1/\sqrt{3}$ according to [107].

In this combined result, $f_{\text{NL}} = 0$ is at just around 2σ , which taken at a face value suggests that the evidence for a significant non-Gaussianity found in 3 year WMAP data by [?] may have been a statistical fluctuation rather than evidence of a real signal.

The results are already sufficiently strong to constrain the ekpyrotic models of generating the primordial structure: these generically predict much higher non-Gaussianity than inflationary models [32]. Following Ref. [34], we parametrize the ekpyrotic model in terms of $\gamma = \dot{\phi}_2/\dot{\phi}_1$ during the phase of creation of entropic perturbations for minimally coupled fields ϕ_i responsible for ekpyrosis and ekpyrotic parameter $\epsilon_{\text{ek}} \gg 1$, the ekpyrotic equivalent of the slow-roll parameter ϵ . In Figure 5 we show our ‘‘Combined’’ constraints on the $n_s - f_{\text{NL}}$ plane together with approximate theoretical predictions [34]:

$$n_s \sim 1 + \frac{2}{\epsilon_{\text{ek}}} - \frac{1}{60} \frac{\log \epsilon_{\text{ek}}}{\log 60}, \quad (47)$$

$$f_{\text{NL}} \sim \frac{4(\gamma^2 - 1)}{\gamma} \epsilon_{\text{ek}} - 85. \quad (48)$$

We note that large parts of parameter space are strongly constrained. For the theoretically preferred value of $\gamma = -1/\sqrt{3}$ [107], ϵ_{ek} is constrained to be between 100 and 10000. Higher values of ϵ_{ek} require considerably lower values of γ and $\gamma \gtrsim -0.3$ is disfavored at 2σ .

Our results are very promising and with this first analysis we already obtain constraints comparable to the best previous constraints. However, we should be cautious

and emphasize that this is only the first application of this new method to the data and there are several issues that require further investigation. While analytically the method is well motivated and can be derived on very general grounds, as shown in Section II C 1, the method needs to be verified further in N -body simulations using large scale tracers comparable to these used in our analysis. Equation (18) has been calibrated with N -body simulations using matter-halo cross-correlation [47]. Auto-correlation analysis of biased halos, which is the basis for the strongest constraints derived here, is typically noisier and has not been verified at the same level of accuracy, although there is no obvious reason why it should give any different results. Still, it would be useful to have larger simulations where the scale dependent bias could be extracted with high significance from auto-correlation analysis. In addition, it would be useful to verify the scaling relations in simulations on samples defined as closely as possible to the real data should be selected, in our case by choosing halos with mean bias of 2 at $z = 0.5$ for the LRG and $b = 2.7$ at $z = 1.7$ for QSO samples.

A second uncertainty has to do with the halo bias dependence on parameters other than halo mass. We have shown that for QSOs we need to allow for the possibility that they are triggered by recent mergers and we have presented extended Press Schechter predictions for the amplitude of the effect in this case, which can affect the limits. To some extent these predictions have been verified using simulations [64], but we do not have a reliable model of populating QSOs inside halos to predict which of the limits is more appropriate for our QSO sample. Moreover, just as the overall halo bias has recently been shown to depend on variables other than the halo mass [66], it is possible that the large scale f_{NL} correction also depends on variables other than the mass and merging history: while we have shown that extended Press-Schechter already predicts the dependence on the merging history, other dependences less amenable to analytic calculations may also exist. It is clear that these issues deserve more attention and we plan to investigate them in more detail in the future using large scale simulations combined with realistic quasar formation models.

On the observational side, there are many possible extensions of our analysis that can be pursued. In this paper we have pursued mostly quasars and luminous red galaxies (LRGs), two well studied and highly biased tracers of large scale structure. On quasar side, we have only analyzed photometric QSO samples split by redshift, but we should be able to obtain better constraints if we also use the luminosity information, specially if brighter quasars are more strongly biased [103]. Moreover, it is worthwhile to apply this analysis also to $z > 3$ spectroscopic quasar sample from SDSS [108], which is very highly biased. Its modelling appears to require almost every massive halo to host a quasar [109], which would reduce the uncertainties related to secondary parameter halo bias dependence. An order of magnitude estimate

shows that small values of f_{NL} do not change mass function enough to affect this deduction. On the LRG side, the most obvious extension of our work would be to pursue the luminosity dependent clustering analysis of the spectroscopic sample. It is well known that LRG clustering amplitude is luminosity dependent [110] and so selecting only brighter LRGs would lead to a higher bias sample and could improve our limits, but ideally one would want to perform the analysis with optimal weighting to minimize the large scale errors as in [93]. Similar type of luminosity dependent analysis could also be done on the LRG photometric sample used here [94].

Finally, with the future data sets from several planned or ongoing surveys, especially those related to the baryonic oscillations most of which use highly biased tracers of large scale structure, a further increase in sensitivity should be possible [47]. The ultimate application of the large-scale clustering method would involve oversampling the 3-dimensional density field in several samples with a range of biases, so that excess clustering due to f_{NL} can be cleanly separated from contamination due to errors in calibration or extinction correction, which are major challenges as one probes below the 1% level. The ultimate sensitivity of the method will likely depend on our ability to isolate these systematics and these should be the subject of future work.

Overall, the remarkably tight constraints obtained from this first analysis on the real data, while still subject to certain assumptions, is a cause of optimism for the future and we expect that the large scale clustering of highly biased tracers will emerge as one of the best methods to search for non-Gaussianity in initial conditions of our universe.

Acknowledgements

We acknowledge useful discussions with Niayesh Afshordi and Dan Babich.

A.S. is supported by the inaugural BCCP Fellowship. C.H. is supported by the U.S. Department of Energy under contract DE-FG03-02-ER40701. N.P. is supported by a Hubble Fellowship HST.HF- 01200.01 awarded by the Space Telescope Science Institute, which is operated by the Association of Universities for Research in Astronomy, Inc., for NASA, under contract NAS 5-26555. Part of this work was supported by the Director, Office of Science, of the U.S. Department of Energy under Contract No. DE-AC02-05CH11231. U.S. is supported by the Packard Foundation and NSF CAREER-0132953 and by Swiss National Foundation under contract 200021-116696/1.

Funding for the Sloan Digital Sky Survey (SDSS) and SDSS-II has been provided by the Alfred P. Sloan Foundation, the Participating Institutions, the National Science Foundation, the U.S. Department of Energy, the National Aeronautics and Space Administration, the Japanese Monbukagakusho, and the Max Planck Society,

and the Higher Education Funding Council for England. The SDSS Web site is <http://www.sdss.org/>.

The SDSS is managed by the Astrophysical Research Consortium (ARC) for the Participating Institutions. The Participating Institutions are the American Museum of Natural History, Astrophysical Institute Potsdam, University of Basel, University of Cambridge, Case Western Reserve University, The University of Chicago, Drexel University, Fermilab, the Institute for Advanced Study, the Japan Participation Group, The Johns Hopkins University, the Joint Institute for Nuclear Astrophysics, the Kavli Institute for Particle Astrophysics and Cosmology, the Korean Scientist Group, the Chinese Academy of Sciences (LAMOST), Los Alamos National Laboratory, the Max-Planck-Institute for Astronomy (MPIA), the Max-Planck-Institute for Astrophysics (MPA), New Mexico State University, Ohio State University, University of Pittsburgh, University of Portsmouth, Princeton University, the United States Naval Observatory, and the University of Washington.

APPENDIX A: WINDOW FUNCTIONS

This appendix describes the computation of the window functions. We begin with a brief revisit of the principles underlying the window function (see the references for more details) and then describe our computational method.

1. Principles

The power spectra in this paper were computed using the methodology of Padmanabhan et al. [111], implemented on the sphere as described in Refs. [94, 112]. The power spectrum is estimated from a vector \mathbf{x} of length N_{pix} containing the galaxy overdensities in each of the N_{pix} pixels. Following the notation of Ref. [94], we estimate the power spectrum in bins,

$$C_\ell = \sum_i p_i \tilde{C}_\ell^i, \quad (\text{A1})$$

where \tilde{C}_ℓ^i is 1 if multipole l is in the i th bin, and 0 otherwise, and p_i are the parameters to be estimated. We can then define the template matrices, \mathbf{C}_i , which are the partial derivatives of the covariance matrix of \mathbf{x} with respect to p_i . The quadratic estimators are then defined:

$$q_i = \frac{1}{2} \mathbf{x}^T \mathbf{C}^{-1} \mathbf{C}_i \mathbf{C}^{-1} \mathbf{x}, \quad (\text{A2})$$

where \mathbf{C} is an estimate of the covariance matrix used to weight the data (our choice is described in Ho et al. [95]). We also build a Fisher matrix,

$$F_{ij} = \frac{1}{2} \text{Tr} (\mathbf{C}^{-1} \mathbf{C}_i \mathbf{C}^{-1} \mathbf{C}_j). \quad (\text{A3})$$

The parameters are then estimated according to

$$p_i = (F^{-1})_{ij} (q_j - \langle q_j \rangle_{\text{noise}}), \quad (\text{A4})$$

where $\langle q_j \rangle_{\text{noise}}$ is the expectation value of q_j for Poisson noise. This is equal to

$$\langle q_j \rangle_{\text{noise}} = \frac{1}{2} \text{Tr} (\mathbf{C}^{-1} \mathbf{C}_i \mathbf{C}^{-1} \mathbf{N}), \quad (\text{A5})$$

where \mathbf{N} is the Poisson noise matrix (i.e. a diagonal matrix with entries equal to the reciprocal of the mean number of galaxies per pixel). This quantity can be computed using the same machinery as used to compute \mathbf{F} .

The actual expectation values of the binned power spectra p_i for a general power spectrum [i.e. not necessarily Equation (A1)] are given by

$$\langle p_i \rangle = (F^{-1})_{ij} (\langle q_j \rangle_{\text{total}} - \langle q_j \rangle_{\text{noise}}); \quad (\text{A6})$$

since signal and noise are uncorrelated this reduces to:

$$\langle p_i \rangle = (F^{-1})_{ij} \langle q_j \rangle_{\text{signal}} = \frac{1}{2} (F^{-1})_{ij} \text{Tr} (\mathbf{C}^{-1} \mathbf{C}_i \mathbf{C}^{-1} \mathbf{S}), \quad (\text{A7})$$

where \mathbf{S} is the signal covariance matrix. Its entries are

$$S_{\alpha\beta} = \sum_\ell C_\ell \sum_{m=-\ell}^\ell Y_{\ell m}(\alpha) Y_{\ell m}^*(\beta), \quad (\text{A8})$$

where α and β are pixels: $1 \leq \alpha, \beta \leq N_{\text{pix}}$. It could also be written as

$$\mathbf{S} = \sum_\ell C_\ell \sum_{m=-\ell}^\ell \mathbf{Y}_{\ell m} \mathbf{Y}_{\ell m}^\dagger, \quad (\text{A9})$$

where $\mathbf{Y}_{\ell m}$ is a vector of length N_{pix} containing the values of the spherical harmonic $Y_{\ell m}$ at each pixel. With some algebra the expectation value collapses down to:

$$\langle p_i \rangle = \sum_\ell W_{i\ell} C_\ell, \quad (\text{A10})$$

where the window function $W_{i\ell}$ is:

$$W_{i\ell} = \frac{1}{2} (F^{-1})_{ij} \sum_{m=-\ell}^\ell \mathbf{Y}_{\ell m}^\dagger \mathbf{C}^{-1} \mathbf{C}_i \mathbf{C}^{-1} \mathbf{Y}_{\ell m}. \quad (\text{A11})$$

2. Computation

Like the other matrix operations with million-pixel maps, direct computation of $W_{i\ell}$ using Equation (A11) is not feasible; it is $O(N_{\text{pix}}^3)$. We have therefore resorted to Monte Carlo methods, analogous to those used for trace estimation, to simultaneously solve for all of the ℓ and m terms in Equation (A11). Define a random vector \mathbf{z} of length N_{pix} and with entries consisting of independent

random numbers ± 1 (i.e. probability 1/2 of being 1 and 1/2 of being -1). Then $\langle \mathbf{z}\mathbf{z}^T \rangle = 1$, so we can write:

$$W_{i\ell} = \frac{1}{2}(F^{-1})_{ij} \left\langle \sum_{m=-\ell}^{\ell} \mathbf{Y}_{\ell m}^\dagger \mathbf{C}^{-1} \mathbf{z} \mathbf{z}^T \mathbf{C}_i \mathbf{C}^{-1} \mathbf{Y}_{\ell m} \right\rangle, \quad (\text{A12})$$

or

$$W_{i\ell} = \frac{1}{2}(F^{-1})_{ij} \left\langle \sum_{m=-\ell}^{\ell} (\mathbf{Y}_{\ell m}^\dagger \mathbf{C}^{-1} \mathbf{z})(\mathbf{Y}_{\ell m}^\dagger \mathbf{C}^{-1} \mathbf{C}_i \mathbf{z}) \right\rangle. \quad (\text{A13})$$

To do a Monte Carlo evaluation of the average, we can take a random vector \mathbf{z} , compute the quantities $\mathbf{C}^{-1}\mathbf{z}$ and $\mathbf{C}^{-1}\mathbf{C}_i\mathbf{z}$. The latter dominates the computation time, as it requires one expensive \mathbf{C}^{-1} operation for each power spectrum bin, but it is also needed in the Monte Carlo evaluation of the Fisher matrix F_{ij} and hence comes with no added cost. The inner product $\mathbf{Y}_{\ell m}^\dagger \mathbf{u}$ for any pixel-space vector \mathbf{u} is the spherical harmonic transform of \mathbf{u} , for which “fast” $O(N_{\text{pix}}^{3/2})$ algorithms exist. We use the implementation of the spherical harmonic transform of Hirata et al. [112].

-
- [1] A. A. Starobinskii, Soviet Journal of Experimental and Theoretical Physics Letters **30**, 682 (1979).
 - [2] A. H. Guth, Phys. Rev. D **23**, 347 (1981).
 - [3] A. D. Linde, Physics Letters B **108**, 389 (1982).
 - [4] A. Albrecht and P. J. Steinhardt, Physical Review Letters **48**, 1220 (1982).
 - [5] E. Komatsu *et al.*, ArXiv e-prints **803**, (2008).
 - [6] V. F. Mukhanov and G. V. Chibisov, Soviet Journal of Experimental and Theoretical Physics Letters **33**, 532 (1981).
 - [7] S. W. Hawking, Physics Letters B **115**, 295 (1982).
 - [8] A. H. Guth and S.-Y. Pi, Physical Review Letters **49**, 1110 (1982).
 - [9] A. A. Starobinskij, Physics Letters B **117**, 175 (1982).
 - [10] J. M. Bardeen, P. J. Steinhardt, and M. S. Turner, Phys. Rev. D **28**, 679 (1983).
 - [11] J. Khoury, B. A. Ovrut, P. J. Steinhardt, and N. Turok, Phys. Rev. D **64**, 123522 (2001).
 - [12] J. Khoury, P. J. Steinhardt, and N. Turok, Physical Review Letters **91**, 161301 (2003).
 - [13] P. J. Steinhardt and N. Turok, Science **296**, 1436 (2002).
 - [14] E. I. Buchbinder, J. Khoury, and B. A. Ovrut, Physical Review Letters **100**, 171302 (2008).
 - [15] A. R. Liddle and A. Mazumdar, Phys. Rev. D **61**, 123507 (2000).
 - [16] S. Gupta, K. A. Malik, and D. Wands, Phys. Rev. D **69**, 063513 (2004).
 - [17] R. Bean, J. Dunkley, and E. Pierpaoli, Phys. Rev. D **74**, 063503 (2006).
 - [18] M. Beltrán, ArXiv e-prints **804**, (2008).
 - [19] E. Komatsu and D. N. Spergel, Phys. Rev. D **63**, 063002 (2001).
 - [20] A. Gangui, F. Lucchin, S. Matarrese, and S. Mollerach, Astrophys. J. **430**, 447 (1994).
 - [21] J. Maldacena, Journal of High Energy Physics **5**, 13 (2003).
 - [22] N. Bartolo, E. Komatsu, S. Matarrese, and A. Riotto, Phys. Rep. **402**, 103 (2004).
 - [23] A. Linde and V. Mukhanov, Phys. Rev. D **56**, 535 (1997).
 - [24] F. Bernardeau and J.-P. Uzan, Phys. Rev. D **66**, 103506 (2002).
 - [25] D. H. Lyth, C. Ungarelli, and D. Wands, Phys. Rev. D **67**, 023503 (2003).
 - [26] G. Dvali, A. Gruzinov, and M. Zaldarriaga, Phys. Rev. D **69**, 023505 (2004).
 - [27] T. Suyama and M. Yamaguchi, Phys. Rev. D **77**, 023505 (2008).
 - [28] K. Enqvist *et al.*, Physical Review Letters **94**, 161301 (2005).
 - [29] K. Enqvist *et al.*, ArXiv High Energy Physics - Phenomenology e-prints (2005).
 - [30] A. Chambers and A. Rajantie, Physical Review Letters **100**, 041302 (2008).
 - [31] A. Jokinen and A. Mazumdar, Journal of Cosmology and Astro-Particle Physics **4**, 3 (2006).
 - [32] P. Creminelli and L. Senatore, Journal of Cosmology and Astro-Particle Physics **11**, 10 (2007).
 - [33] J.-L. Lehners and P. J. Steinhardt, Phys. Rev. D **77**, 063533 (2008).
 - [34] J.-L. Lehners and P. J. Steinhardt, ArXiv e-prints **804**, (2008).
 - [35] E. Komatsu *et al.*, Astrophys. J. Supp. **148**, 119 (2003).
 - [36] P. Creminelli, L. Senatore, M. Zaldarriaga, and M. Tegmark, Journal of Cosmology and Astro-Particle Physics **3**, 5 (2007).
 - [37] T. H. Jarrett *et al.*, Astron. J. **119**, 2498 (2000).
 - [38] E. Jeong and G. F. Smoot, ArXiv e-prints **710**, (2007).
 - [39] C. Hikage *et al.*, ArXiv e-prints **802**, (2008).
 - [40] A. Cooray, D. Sarkar, and P. Serra, ArXiv e-prints **803**, (2008).
 - [41] A. Cooray, C. Li, and A. Melchiorri, Phys. Rev. D **77**, 103506 (2008).
 - [42] R. Scoccimarro, E. Sefusatti, and M. Zaldarriaga, Phys. Rev. D **69**, 103513 (2004).
 - [43] F. Lucchin, S. Matarrese, and N. Vittorio, Astron. Astrophys. **162**, 13 (1986).
 - [44] S. Matarrese, L. Verde, and R. Jimenez, Astrophys. J. **541**, 10 (2000).
 - [45] J. Robinson and J. E. Baker, Mon. Not. R. Astron. Soc. **311**, 781 (2000).
 - [46] A. J. Benson, C. Reichardt, and M. Kamionkowski, Mon. Not. R. Astron. Soc. **331**, 71 (2002).
 - [47] N. Dalal, O. Doré, D. Huterer, and A. Shirokov, Phys. Rev. D **77**, 123514 (2008).
 - [48] J. M. Bardeen, J. R. Bond, N. Kaiser, and A. S. Szalay, Astrophys. J. **304**, 15 (1986).
 - [49] R. K. Sheth and G. Tormen, Mon. Not. R. Astron. Soc. **308**, 119 (1999).
 - [50] W. H. Press and P. Schechter, Astrophys. J. **187**, 425 (1974).
 - [51] S. Cole and N. Kaiser, Mon. Not. R. Astron. Soc. **237**,

- 1127 (1989).
- [52] S. Matarrese and L. Verde, *Astrophys. J. Lett.* **677**, L77 (2008).
- [53] E. Hatziminaoglou *et al.*, *Mon. Not. R. Astron. Soc.* **343**, 692 (2003).
- [54] P. F. Hopkins, L. Hernquist, T. J. Cox, and D. Kereš, *Astrophys. J. Supp.* **175**, 356 (2008).
- [55] T. Urrutia, M. Lacy, and R. H. Becker, *Astrophys. J.* **674**, 80 (2008).
- [56] S. R. Furlanetto and M. Kamionkowski, *Mon. Not. R. Astron. Soc.* **366**, 529 (2006).
- [57] A. R. Wetzel *et al.*, *Astrophys. J.* **656**, 139 (2007).
- [58] C. Lacey and S. Cole, *Mon. Not. R. Astron. Soc.* **262**, 627 (1993).
- [59] M. R. Santos, V. Bromm, and M. Kamionkowski, *Mon. Not. R. Astron. Soc.* **336**, 1082 (2002).
- [60] A. J. Benson, M. Kamionkowski, and S. H. Hassani, *Mon. Not. R. Astron. Soc.* **357**, 847 (2005).
- [61] N. Dalal, M. White, J. R. Bond, and A. Shirokov, *ArXiv e-prints* **803**, (2008).
- [62] J. D. Cohn, J. S. Bagla, and M. White, *Mon. Not. R. Astron. Soc.* **325**, 1053 (2001).
- [63] J. D. Cohn and M. White, *Astroparticle Physics* **24**, 316 (2005).
- [64] O. Fakhouri and C.-P. Ma, *Mon. Not. R. Astron. Soc.* **386**, 577 (2008).
- [65] V. Springel *et al.*, *Nature (London)* **435**, 629 (2005).
- [66] L. Gao, V. Springel, and S. D. M. White, *Mon. Not. R. Astron. Soc.* **363**, L66 (2005).
- [67] R. H. Wechsler *et al.*, *Astrophys. J.* **652**, 71 (2006).
- [68] Y. P. Jing, Y. Suto, and H. J. Mo, *Astrophys. J.* **657**, 664 (2007).
- [69] L. Gao and S. D. M. White, *Mon. Not. R. Astron. Soc.* **377**, L5 (2007).
- [70] A. Lewis and S. Bridle, *Phys. Rev. D* **66**, 103511 (2002).
- [71] G. Hinshaw *et al.*, *Astrophys. J. Supp.* **170**, 288 (2007).
- [72] L. Page *et al.*, *Astrophys. J. Supp.* **170**, 335 (2007).
- [73] K. Grainge *et al.*, *Mon. Not. R. Astron. Soc.* **341**, L23 (2003).
- [74] C. L. Kuo *et al.*, *Astrophys. J.* **664**, 687 (2007).
- [75] A. C. S. Readhead *et al.*, *Astrophys. J.* **609**, 498 (2004).
- [76] P. Astier *et al.*, *Astron. Astrophys.* **447**, 31 (2006).
- [77] M. Fukugita *et al.*, *Astron. J.* **111**, 1748 (1996).
- [78] D. G. York *et al.*, *Astron. J.* **120**, 1579 (2000).
- [79] D. W. Hogg, D. P. Finkbeiner, D. J. Schlegel, and J. E. Gunn, *Astron. J.* **122**, 2129 (2001).
- [80] J. E. Gunn *et al.*, *Astron. J.* **131**, 2332 (2006).
- [81] J. E. Gunn *et al.*, *Astron. J.* **116**, 3040 (1998).
- [82] J. A. Smith *et al.*, *Astron. J.* **123**, 2121 (2002).
- [83] D. L. Tucker *et al.*, *Astronomische Nachrichten* **327**, 821 (2006).
- [84] N. Padmanabhan *et al.*, *Astrophys. J.* **674**, 1217 (2008).
- [85] J. R. Pier *et al.*, *Astron. J.* **125**, 1559 (2003).
- [86] Ž. Ivezić *et al.*, *Astronomische Nachrichten* **325**, 583 (2004).
- [87] M. A. Strauss *et al.*, *Astron. J.* **124**, 1810 (2002).
- [88] D. J. Eisenstein *et al.*, *Astron. J.* **122**, 2267 (2001).
- [89] G. T. Richards *et al.*, *Astron. J.* **123**, 2945 (2002).
- [90] M. R. Blanton *et al.*, *Astron. J.* **125**, 2276 (2003).
- [91] J. K. Adelman-McCarthy *et al.*, *Astrophys. J. Supp.* **175**, 297 (2008).
- [92] J. K. Adelman-McCarthy *et al.*, *Astrophys. J. Supp.* **162**, 38 (2006).
- [93] M. Tegmark *et al.*, *Phys. Rev. D* **74**, 123507 (2006).
- [94] N. Padmanabhan *et al.*, *Mon. Not. R. Astron. Soc.* **378**, 852 (2007).
- [95] S. Ho *et al.*, *ArXiv e-prints* **801**, (2008).
- [96] J. J. Condon *et al.*, *Astron. J.* **115**, 1693 (1998).
- [97] S. Cole *et al.*, *Mon. Not. R. Astron. Soc.* **362**, 505 (2005).
- [98] R. Mandelbaum and U. Seljak, *Journal of Cosmology and Astro-Particle Physics* **6**, 24 (2007).
- [99] N. Padmanabhan, M. White, P. Norberg, and C. Porciani, *ArXiv e-prints* **802**, (2008).
- [100] C. M. Hirata *et al.*, *ArXiv e-prints* **801**, (2008).
- [101] G. T. Richards *et al.*, *Astrophys. J. Supp.* **155**, 257 (2004).
- [102] M. A. Weinstein *et al.*, *Astrophys. J. Supp.* **155**, 243 (2004).
- [103] C. Porciani and P. Norberg, *Mon. Not. R. Astron. Soc.* **371**, 1824 (2006).
- [104] J. R. Bond, A. H. Jaffe, and L. Knox, *Astrophys. J.* **533**, 19 (2000).
- [105] R. K. Sachs and A. M. Wolfe, *Astrophys. J.* **147**, 73 (1967).
- [106] T. Giannantonio *et al.*, *Phys. Rev. D* **77**, 123520 (2008).
- [107] J.-L. Lehners and N. Turok, *Phys. Rev. D* **77**, 023516 (2008).
- [108] Y. Shen *et al.*, *Astron. J.* **133**, 2222 (2007).
- [109] M. White, P. Martini, and J. D. Cohn, *ArXiv e-prints* **711**, (2007).
- [110] W. J. Percival *et al.*, *Astrophys. J.* **657**, 645 (2007).
- [111] N. Padmanabhan, U. Seljak, and U. L. Pen, *New Astronomy* **8**, 581 (2003).
- [112] C. M. Hirata *et al.*, *Phys. Rev. D* **70**, 103501 (2004).

